

# Effect of plastic coating on the density of plasma formed in Si foil targets irradiated by ultra high-contrast relativistic laser pulses

A. S. Martynenko,<sup>1,2</sup> S.A. Pikuz,<sup>1,2,\*</sup> I. Yu. Skobelev,<sup>1,2</sup> S. N. Ryazantsev,<sup>1,2</sup> C. Baird,<sup>3</sup> N. Booth,<sup>4</sup> L. Doehl,<sup>3</sup> P. Durey,<sup>3</sup> A. Ya. Faenov,<sup>1,5</sup> D. Farley,<sup>3</sup> R. Kodama,<sup>5,6</sup> K. Lancaster,<sup>3</sup> P. McKenna,<sup>7</sup> C. D. Murphy,<sup>3</sup> C. Spindloe,<sup>4</sup> T. A. Pikuz,<sup>1,5</sup> and N. Woolsey<sup>3</sup>

<sup>1</sup> *Joint Institute for High Temperatures of Russian Academy of Sciences, 125412 Moscow, Russia*

<sup>2</sup> *National Research Nuclear University MEPhI, Kashirskoe Sh. 31, 115409 Moscow, Russia*

<sup>3</sup> *York Plasma Institute, Department of Physics, University of York, York YO10 5DD, UK*

<sup>4</sup> *Central Laser Facility, STFC Rutherford Appleton Laboratory, Didcot OX11 0QX, UK*

<sup>5</sup> *Open and Transdisciplinary Research Initiative, Osaka University, Osaka 565-0871, Japan*

<sup>6</sup> *Institute of Laser Engineering, Osaka University, Suita 565-0871, Japan*

<sup>7</sup> *Department of Physics, SUPA, University of Strathclyde, Glasgow G4 0NG, UK*

\* spikuz@gmail.com

The formation of high energy density matter occurs in inertial confinement fusion, astrophysical, and geophysical systems. In this context, it is important to couple as much energy as possible into a target whilst maintaining high density. A recent experimental campaign, using buried layer (or a “sandwich” type) targets and the ultra-high laser contrast Vulcan petawatt laser facility results in 500 Mbar pressures in solid density plasmas (which corresponds to about  $4.6 \times 10^7$  J/cm<sup>3</sup> of energy density). The densities and temperatures of the generated plasma were measured based on the analysis of X-ray spectral lines profiles and relative intensities.

## I. INTRODUCTION

Studies of high energy density matter (>1 Mbar, 100 GPa,  $10^{11}$  J/m<sup>3</sup>) have been of great interest for various fields of science, such as astrophysics, physics of plasma, thermonuclear fusion and particle acceleration technologies [1]. Different methods based on the compression and heating of matter by shock waves (for example, generated by gas guns, pinch discharges, high-power lasers) are commonly used to create such states under laboratory conditions. If a material is heated almost instantaneously, for example by using a sufficiently short duration heating source, then the compression stage might be unnecessary. Using this isochoric approach, it is relatively easy to achieve high energy

density conditions using short-pulse lasers at relativistic intensities [2–6].

It is of fundamental importance to know the plasma conditions as laser energy is deposited into a target and this is particularly challenging when a laser pulse has a sufficiently intense prepulse. In the case of a laser with a poor contrast ratio, the prepulse forms an extended region of plasma with densities below the critical density [7]. This means that isochoric formation of high energy density matter close to solid density is not possible where the contrast ratio (i.e. ratio of the laser peak intensity to the intensity of pulse pedestal) exceeds  $10^{12}$  [6]. Furthermore, laser technology improvements (resulting in intensities exceeding  $10^{23}$  W/cm<sup>2</sup>) will require ever higher laser contrast.

The characteristic time between the front of the intense laser pedestal and the main laser pulse is about 10 ps [17]. Taking preplasma expansion speed to be  $v_{exp} \sim 10^6\text{-}10^7$  cm/s (which is of the order of the speed of sound), and the skin layer thickness  $l_0 \sim 0.1$   $\mu\text{m}$  (for a laser wavelength of 1  $\mu\text{m}$ ), one can estimate that the preplasma volume increases in about 2-10 times before the main laser pulse arrival. In other words, the main energy of the heating laser pulse is deposited in a target with a density which is significantly lower than the solid state one because of the intense laser pedestal. Coating is supposed to significantly increase the lifetime of the solid-state preplasma. A transparent coating layer deposited on the front or on both target surfaces may prevent the expansion of the preplasma keeping the target density close to the solid-state one, at least at picosecond time scale.

In general, the formation of preplasma is not problematic unless the preplasma expansion significantly affects the target of interest. One solution is to delay the impact of preplasma expansion by sandwiching the material of interest in a multi-layered target, known as tamping.

The implementation of target coating and tamping in laser-matter interaction experiments has a substantial background. Plastic absorbing coatings have been used as a compressor for spherical thermonuclear target in inertial confinement studies since the early 70s [8,9]. At the same time, experiments on the laser irradiation of coated (layered) solid targets began [10–12]. Much later, it was proposed to use laser transparent target coatings to prevent a preplasma formation by a pre-pulse of a powerful pico- or femtosecond laser pulse [13–16].

The outer layer of the target is usually formed from material with a higher ionisation threshold than the inner material and is also transparent to laser radiation. As the laser prepulse intensity increases any preplasma at

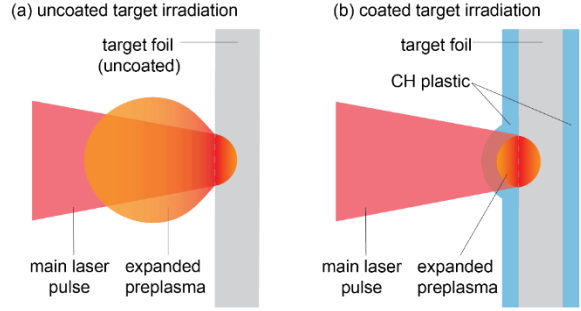


FIG. 1. Schematic comparison of an intense laser pulse interacting with a solid density target and the formation of preplasma on the target surface in case of (a) plain foil target and (b) sandwich type target (a preplasma forms at the inner interface between the outer and inner layer in a sandwich target).

the interface between the outer and inner layers, as is illustrated in FIG. 1 (b), is confined by the inertia of the outer layer. This impedes the expansion of the plasma of interest, helping to maintain a high density ideally until the arrival of the main pulse. The use of a sandwich targets demands a high laser contrast, yet in general, the requirements for the laser contrast are noticeably lower.

Contrast measurements of high-contrast lasers are difficult to make, and it is almost impossible to *a priori* predict the laser contrast for each laser shot. Here we use X-ray spectroscopy to study high-contrast laser interactions with sandwich targets up to laser intensities of  $6 \times 10^{20}$  W/cm<sup>2</sup>. We compare emission from plain foil targets and sandwich targets, and find that the use of sandwich targets allows the material to remain close to a solid density with an energy density of about  $5 \times 10^7$  J/cm<sup>3</sup> or 500 Mbar.

## II. EXPERIMENTAL DATA

The experiment was conducted on the Vulcan Nd : glass (with a wavelength of 1054 nm) petawatt laser system at the Rutherford-Appleton laboratory (UK) [17]. For each shot, the p-polarized laser beam delivered  $\sim 300$  J on the target in  $\sim 1$  ps pulse and was focused onto a target using an f/3 off-axis parabola. This produced a focal spot

1 containing approximately 30% of the energy  
2 in a  $7\text{ }\mu\text{m}$  diameter region. Using OPCPA [1]  
3 and a plasma mirror [18–20] placed just  
4 before the focal plane, the laser contrast  
5 exceeded  $10^{10}$  at 1 ns [21]. See the top view  
6 of experimental setup in FIG. 2. The angle of  
7 incidence of laser to the target surface was  
8  $45^\circ$ . We compare the X-ray emission from  
9 plain and CH plastic-coated  $\mu\text{m}$ -thick solid Si  
10 foils using three focusing spectrometers with  
11 spatial resolution (FSSR) [22,23]. The  
12 spectrometers recorded emission at  $\sim 5^\circ$  to the  
13 target surface normal (see FIG. 2) with  
14 spherically-bent quartz crystals and image  
15 plate detectors. These spectrometers were  
16 designed to record spectral emission at high  
17 resolution across from different parts of the  
18 spectrum and to cover a continuous yet broad  
19 spectral range that extends from 4.5 to  $7.5\text{ }\text{\AA}$   
20 as summarised in TABLE I.

21 TABLE I. Spectral ranges of each FSSR is described  
22 experiment.

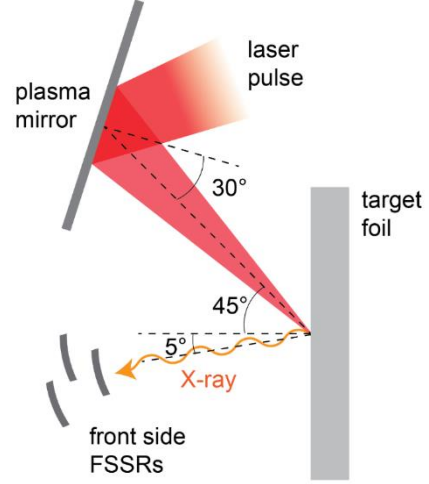


FIG. 2. Experimental schematic showing the relative positions of the target foil, laser pulse, plasma mirror and the three FSSR spectrometers.

Spectrometer number	1	2	3
Spectral range, $\text{\AA}$	4.5-5.8	5.5-6.9	6.6-7.5

23 Overlapping the spectral ranges of each  
24 spectrometer enables cross-calibration of

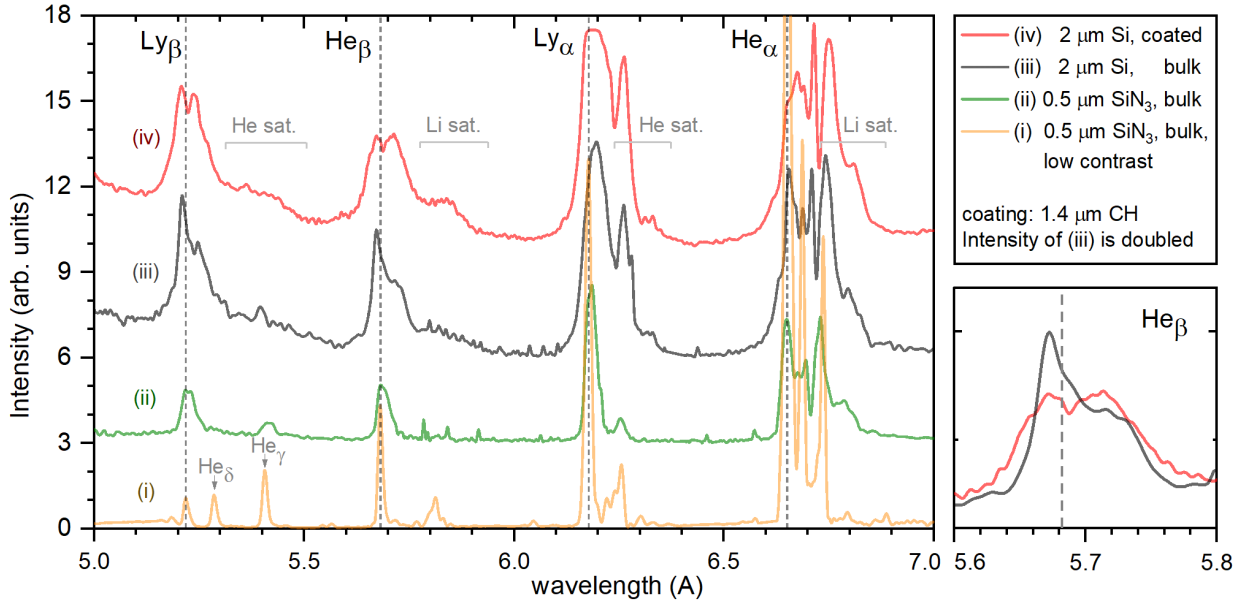


FIG. 3 Experimental X-ray spectra obtained by laser pulse irradiation of a (i)  $0.5\text{ }\mu\text{m}$   $\text{SiN}_3$  uncoated foil (orange curve) without plasma mirror, (ii)  $0.5\text{ }\mu\text{m}$   $\text{SiN}_3$  uncoated foil (green curve) with plasma mirror, (iii)  $2\text{ }\mu\text{m}$  Si foil coated on both sides with  $1.4\text{ }\mu\text{m}$  CH plastic layers (red curve), and (iv)  $2\text{ }\mu\text{m}$  Si uncoated foil (black curve). For ease of comparison, the intensity of the curve (i) divided by factor 2; and the intensity of the curve (iii) was increased by 2 times.

spectral intensities as well as the facility to accurately identify and subtract bremsstrahlung contribution in the measurement. A more detailed description of the experiment is contained in Ref. [18].

The four spectra in FIG. 3 are from (i) a low contrast laser interaction with a 0.5  $\mu\text{m}$  thick SiN target and in (ii) to (iv) high contrast interactions with 0.5  $\mu\text{m}$  thick SiN, 2  $\mu\text{m}$  thick Si, and 2  $\mu\text{m}$  thick Si targets coated with 1.4  $\mu\text{m}$  thick CH plastic respectively. Data extraction for all spectra uses same methodology. The spectra are space and time integrated and the emission is dominated by the densest and hottest region of the plasma. The low contrast measurement, spectrum (i), used a standard mirror in place of the plasma mirror. This mirror reflects most of the laser prepulse and the target foil expands. As a result, the main part of the laser pulse heats an extended low-density plasma. There is a clear signature of this in the emission spectrum which is characterized by relatively narrow and well distinguished lines from silicon H- and He-like ions and associated satellites. Further analysis show that the spectral line widths are consistent with a near critical density plasma. The narrow spectral lines allow the use of this spectrum to verify and accurately set the dispersion of the three spectrometers and then as a reference enabling the precise determination of the spectral line positions in all spectra. The spectral line centres of the Si XIV ( $\text{Si}^{13+}$ )  $\text{Ly}_\alpha$ ,  $\text{Ly}_\beta$  lines and Si XIII ( $\text{Si}^{12+}$ )  $\text{He}_\alpha$ ,  $\text{He}_\beta$  are shown by the vertical dashed lines. In addition, the  $\text{He}_\gamma$  and  $\text{He}_\delta$  resonance lines are clearly resolved in spectrum (i).

In spectrum (ii) the high contrast laser interacts with a 0.5  $\mu\text{m}$  SiN<sub>3</sub> foil and the spectral lines are much broader than in spectrum (i). The spectral resonance lines appear to broaden to long wavelength side of the resonance line centres. This broadening is characteristic of a higher density plasma and results from a combination of increased Stark

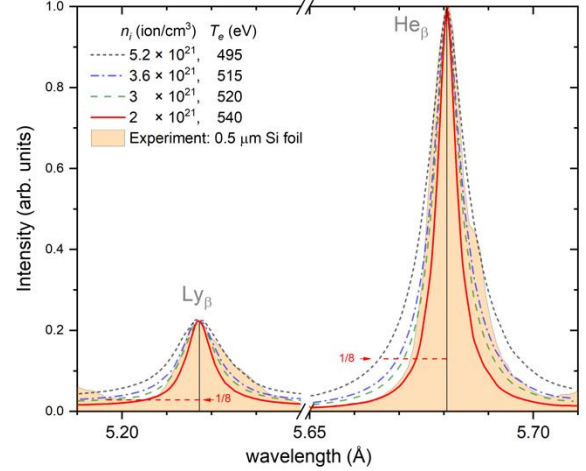


FIG. 4 Comparison of numerically calculated and experimental spectra (an orange area) for  $\text{Ly}_\beta$  and  $\text{He}_\beta$  lines emitted by the 0.5  $\mu\text{m}$  SiN<sub>3</sub> foil during irradiation by a high contrast laser beam (plasma mirror was not used). The spectra are modelled for different initial plasma parameters (colour curves) in the approximation of plasma adiabatic expansion approach (initial plasma parameters are presented in the legend); solid line represents the best-fit.

broadening and increasing recombination rate that populates the satellite states. Dense plasma effects result in similar line intensities in the Ly-like and He-like series and disappearance of the  $\text{He}_\delta$  line. The spectral lines remain clearly resolved and this indicates that the plasma density is higher than critical density but lower than solid.

Increasing the thickness of a target results in more hot material remaining at near solid density during the laser interaction, as a result emission may be dominated by a plasma of higher density. Spectrum (iii) is from a 2  $\mu\text{m}$  thick Si foil and shows strong emission from  $\text{Ly}_\alpha$ ,  $\text{Ly}_\beta$  and  $\text{He}_\alpha$ ,  $\text{He}_\beta$  lines. These lines are broader than spectral lines observed in spectrum (ii), satellite structure on the long wavelength side of these lines is more prominent with this structure extending towards the adjacent resonance line. As a result, the spectral lines are not as well resolved. For example,  $\text{He}_\beta$  transition line is partially overlapped with He-like satellites to  $\text{Ly}_\beta$  transition line in a region of 5.5-5.7 Å. The asymmetry of the spectral line profiles



close to the line centres (indicated by the vertical dashed line) is indicative of self-absorption in the plasma. For example, the optical mean-free-path of  $\text{Ly}\beta$  radiation is comparable to the  $2\text{ }\mu\text{m}$  thickness of the target, i.e. an optical depth of approximately one.

The fourth spectrum (iv) is from  $2\text{ }\mu\text{m}$  Si foil with a  $1.4\text{ }\mu\text{m}$  outer layer of CH plastic on both front and rear sides. Here the spectral lines are broad and overlapping, with rather symmetrical  $\text{Ly}\beta$  and  $\text{He}\beta$  line profiles, in comparison the  $\text{Ly}\alpha$  and  $\text{He}\alpha$  are optically thick and strongly modified by opacity effects. The central dip close to the line centre of the  $\text{Ly}\beta$  and  $\text{He}\beta$  transitions is caused by the self-absorption. A comparison of the integrated spectral intensity in these spectral lines across spectra (ii), (iii) and (iv) show the emission is greatest from sandwich target. This results from the inertial tamping of the target by the plastic layer and increased density.

There is a noticeable shift of  $\text{Ly}\beta$ ,  $\text{He}\beta$  line positions in spectra (ii), (iii), and (iv) compared to spectra (i), this is likely due to the compression of electron energy levels and by a decrease in the energy of the photons emitted in a dense plasma, which was discussed in Ref. [24]. The consistency of the effect was confirmed by the examination of several targets with slightly different coatings and thicknesses of the main foil.

### III. NUMERICAL SIMULATION AND DATA ANALYSIS

Quantitative assessment of plasma parameters, relies upon atomic and plasma synthesis models, here we compare measurement with the radiation-collisional kinetic code PrismSPECT [25,26].

As discussed above, a preliminary analysis suggests near-solid plasma density in cases (iii) and (iv). The conditions of near-solid density and high temperature occur shortly after the arrival of the main laser

pulse, this results in the most significant contribution to the total spectrum. Here, the modelling of the emission spectrum uses a stationary approximation, we demonstrate this is sufficient to describe the experimental data below. In comparison, in case (i) a prepulse (as the laser is used without a plasma mirror) forms a preplasma from the uncoated target. This preplasma expands significantly before the arrival of the main laser pulse. This leads to absorption of the intense laser pulse energy in a plasma of noticeably lower density. We find the analysis of case (i) must include the plasma expansion as well as late stages in the plasma evolution to simulate the spatially and time-integrated spectrum.

#### A. THIN UNCOATED TARGET

A numerical simulation of  $\text{Ly}\beta$  and  $\text{He}\beta$  spectral lines was performed according to an adiabatic expansion approach developed in Ref. [27]. Comparison of the calculated spectra with experimental one was performed as shown in FIG. 4.

The  $\text{Ly}\beta$  and  $\text{He}\beta$  spectral line have low opacity with widths that are sensitive to variations of plasma parameters and line broadening is most easily seen in the wings of the profile, where the emission from initial stages of plasma expansion makes the major contribution. Thus, it is more advantageous to compare the model and experimental line profiles at the lowest possible relative intensities, to ensure accurate evaluation of plasma density evaluation during the initial stages of the expansion. This possible at the  $1/8$  level of the spectral line maxima due to the low level of the noise in the experiment. There is clear asymmetry of the spectral line profile with the red wing broadened by satellite transitions. Resonant line ( $\text{Ly}\beta$  and  $\text{He}\beta$ ) profiles analysis uses the blue (short-wavelength) wing of each line. This approach gives an ion and electron density of  $2(\pm 0.5) \times 10^{21}\text{ ion/cm}^3$  and  $2.5(\pm 0.5) \times 10^{22}\text{ electron/cm}^3$  respectively, and temperature of

1 about 520 eV, this is shown as the red solid  
2 curve in FIG. 4 with an average energy  
3 density in a range of  $2(\pm 0.5) \times 10^6$  J/cm<sup>3</sup>. The  
4 estimated plasma density is more than one  
5 order of magnitude lower than solid density.  
6 At these densities, the emission lines will  
7 have negligible line centre shifts; the  
8 spectrum from case (i) is used as a reference  
9 spectrum. The dot-dashed curves in FIG. 4  
10 illustrate the data quality and the precision of  
11 the lines shape comparisons.

## 12 B. THICK COATED AND UNCOATED 13 TARGETS

14 High, near solid density, is expected in  
15 cases (iii) and (iv) which use a very high  
16 contrast laser pulse and thick and buried  
17 targets respectively. Using a homogeneous  
18 and stationary approximation (i.e. time  
19 constant single density and temperature). It is  
20 possible to find a good match between the  
21 model and experimental spectra. This is  
22 clearly demonstrated across a wide spectral  
23 range (4.8-7 Å) for the thick bulk target case  
24 (iii) in FIG. 5 (a) and for the buried layer case  
25 (iv) in FIG. 5 (b). To determine the range of

26 possible plasma parameters, we varied the  
27 model plasma density temperature, and  
28 thickness values in respect to the best-fit  
29 curves checking when deviation between  
30 model and experimental spectra becomes  
31 significant. We used  $\text{Ly}_\alpha/\text{Ly}_\beta$  and  $\text{He}_\beta/\text{Ly}_\beta$   
32 lines intensities ratios, widths of  $\text{Ly}_\beta$  and  $\text{He}_\beta$   
33 to estimate plasma density (and thickness), as  
34 illustrated in FIG. 6 for a 2 µm silicon coated  
35 target. Of all the mentioned, only the  $\text{He}_\beta/\text{Ly}_\beta$   
36 ratio shows a significant temperature  
37 dependence, which allows us to estimate not  
38 only the plasma density but also its  
39 temperature, as shown in FIG. 6 c. The model  
40 curves were obtained for a fixed plasma  
41 thickness of 2 and 3 µm, but other values were  
42 considered as well. Color areas show possible  
43 ranged of ion density estimated from  
44 experiment. One can see that there is its  
45 intersection for 2 µm plasma thickness (FIG.  
46 6 a), but a good one for 3 µm (FIG. 6 b).  
47 Dash lines in FIG. 5 show how the data  
48 quality enables accurate determination of the  
49 plasma density. There are differences  
50 between the modeled and experiment line  
51 shapes. These differences are mainly due to

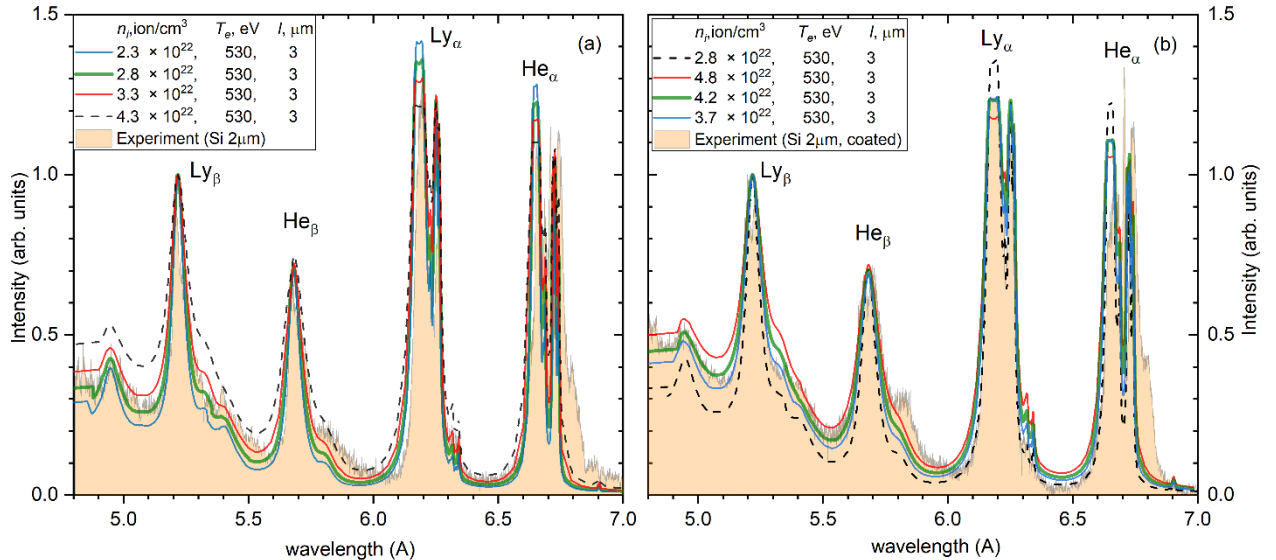


FIG. 5. Simulation data calculated in the stationary approximation (coloured lines) in comparison with experimental spectra (orange regions) for (a) an uncoated 2 µm Si foil, case (iii), and (b) 1.4 µm CH + 2 µm Si + 1.4 µm CH, case (iv). Solid green lines are best-fits; red and blue curves are over- and under-estimations respectively. The ion density, electron temperature, and plasma thickness denoted by  $n_i$ ,  $T_e$ , and  $l$  respectively are given in the legend.

1 He-like satellites of  $\text{Ly}_\alpha$  and  $\text{Ly}_\beta$  as well as Li-  
2 like satellites of  $\text{He}_\alpha$  and  $\text{He}_\beta$  transition lines.  
3 Emission from these satellites is stronger at  
4 lower temperature suggesting this spectral  
5 component comes from material at a lower  
6 temperature. We suggest these satellites  
7 originate from material in the regions around  
8 the laser spot and from late stages of the  
9 experiment after the main laser and as the  
10 plasma expands and cools. Peripheral or late  
11 stages plasma was relatively cold or less  
12 dense, so they were sufficiently less  
13 contributing to the integrated experimental  
14 spectra [27]. It causes some underestimation  
15 of plasma density and temperature.  
16 Therefore, ranges of 5.4-5.6 Å, 5.75-6 Å, and  
17 6.75-7 Å of experimental spectra are not well  
18 described in the modelling.

19 Our comparison of the resonance line  
20 transitions in the model and experimental  
21 spectra suggest peak ion and electron  
22 densities, and temperature, of  $2.8(\pm 0.5) \times 10^{22}$   
23  $\text{ion}/\text{cm}^3$ ,  $3.6(\pm 0.6) \times 10^{23}$   $\text{electron}/\text{cm}^3$ ,  
24 520-540 eV respectively and a plasma  
25 thickness of 3-3.3  $\mu\text{m}$  for spectrum (iii). The  
26 nominal target thickness was 2  $\mu\text{m}$  of  
27 uncoated Si. The average energy density for  
28 this plasma parameters is  
29  $3.1(\pm 0.5) \times 10^7 \text{ J}/\text{cm}^3$ .

30 The spectrum (iii) shows spectral line  
31 shifts, which are probably dense plasma  
32 effects not included in the PrismSPECT code,  
33 therefore they were accounted by a manual  
34 shifting of wavelengths of  $\text{Ly}_\beta$ ,  $\text{He}_\beta$  lines of  
35 calculated spectra using the approach  
36 implemented in Ref. [24].  $\text{He}_\beta/\text{Ly}_\beta$  ratio  
37 shows strong dependence on plasma  
38 density [27].

39 Model comparisons with the  
40 experimental spectrum (iv) suggests ion and  
41 electron densities of  $4.2(\pm 0.5) \times 10^{22} \text{ ion}/\text{cm}^3$   
42 and  $5.4(\pm 0.6) \times 10^{23} \text{ electron}/\text{cm}^3$   
43 respectively. The temperature and thickness  
44 are 520-540 eV and 2.8-3.1  $\mu\text{m}$  respectively.  
45 This gives an average energy density of  
46  $4.6(\pm 0.5) \times 10^7 \text{ J}/\text{cm}^3$ . The inferred plasma

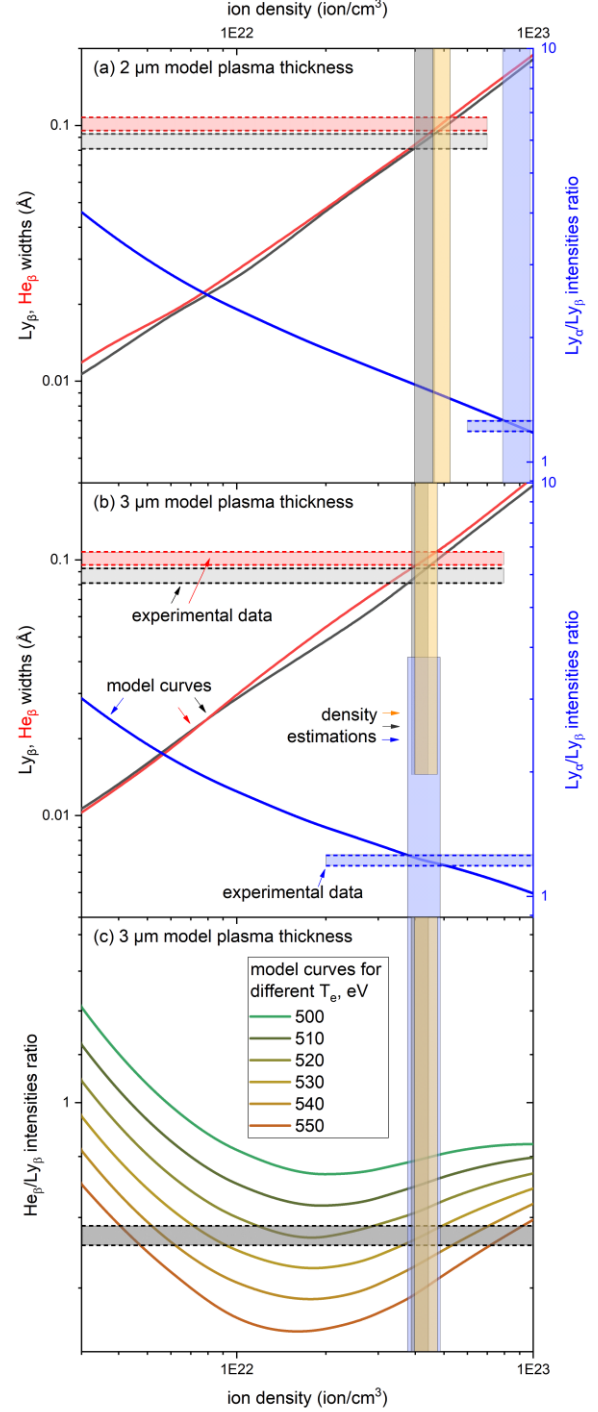


FIG. 6. Comparison of model curves (for different plasma thickness) and experimental data (2  $\mu\text{m}$  silicon coated target), namely, widths of  $\text{Ly}_\beta$  line (black curve in fig. a and b) and  $\text{He}_\beta$  line (red curve in fig. a and b), lines intensity ratios of  $\text{Ly}_\alpha/\text{Ly}_\beta$  (blue curve in fig. b) and  $\text{He}_\beta/\text{Ly}_\beta$  (colour curves in fig. c).

1 densities for cases (iii) and (iv) are close to  
2 the solid-state density. This indicates that  
3 there was no significant preplasma or target  
4 expansion prior to the interaction with the  
5 main laser pulse. Furthermore, the plasma  
6 density of the plastic-coated target, case (iv),  
7 is higher than the uncoated target, case (iii).  
8 Therefore, the use of a plastic layer increases  
9 the plasma confinement.

#### IV. CONCLUSION

11 In this paper, we experimentally  
12 studied time-integrated X-ray emission  
13 spectra of 2 and 0.5  $\mu\text{m}$  Si foils irradiated  
14 with ultra-high contrast relativistic intensities  
15 laser beams of the Vulcan petawatt facility  
16 (UK). We compared spectra for coated (with  
17 CH plastic) and uncoated targets; for high and  
18 ultra-high laser contrast cases. An analysis of  
19 relative heights and profiles of spectral lines  
20 and comparison with numerical spectra of a  
21 radiation-collisional kinetic code allows to  
22 distinguish plasma with quite close  
23 parameters. Based on that, it was confirmed  
24 that irradiation of a few- $\mu\text{m}$ -thick bulk solid  
25 target with the ultra-high contrast laser can  
26 generate a hot plasma only a factor of two or  
27 three lower than solid density. We find that  
28 only the use of targets buried in  $\mu\text{m}$ -thick  
29 plastic layers can ensure even higher  
30 densities, up to near-solid, which is of a great  
31 interest in high energy density experiments.  
32 Correspondingly, silicon dense plasma states  
33 were obtained with an energy density of  
34 about  $4.6 \times 10^7 \text{ J/cm}^3$ , ion density of  
35  $4.2(\pm 0.5) \times 10^{22} \text{ ion/cm}^3$ , which is 0.8-0.9 of  
36 the solid density.

37 Thus, in this work, we proposed and  
38 tested the approach based on the X-ray  
39 emission spectral diagnostic that allows us to  
40 estimate the plasma density of coated targets.  
41 The use of sandwich type targets allows to  
42 ensure the conditions of isochoric heating.

#### ACKNOWLEDGMENTS

The work is done under financial  
support of Russian Science Foundation (grant  
#17-72-20272). The work of UK team  
received financial support from UK EPSRC  
grants [EP/L01663X/1](#) and [EP/H012605/1](#).

#### REFERENCES

- [1] G. A. Mourou, T. Tajima, and S. V. Bulanov, *Rev. Mod. Phys.* **78**, 309 (2006).
- [2] J. H. Sung, H. W. Lee, J. Y. Yoo, J. W. Yoon, C. W. Lee, J. M. Yang, Y. J. Son, Y. H. Jang, S. K. Lee, and C. H. Nam, *Opt. Lett.* **42**, 2058 (2017).
- [3] S. Gales, K. A. Tanaka, D. L. Balabanski, F. Negoita, D. Stutman, O. Tesileanu, C. A. Ur, D. Ursescu, I. Andrei, S. Ataman, M. O. Cernaianu, L. D'Alessi, I. Dancus, B. Diaconescu, N. Djourellov, D. Filipescu, P. Ghenuche, D. G. Ghita, C. Matei, K. Seto, M. Zeng, and N. V. Zamfir, *Reports Prog. Phys.* **81**, 094301 (2018).
- [4] D. N. Papadopoulos, P. Ramirez, K. Genevrier, L. Ranc, N. Lebas, A. Pellegrina, C. Le Blanc, P. Monot, L. Martin, J. P. Zou, F. Mathieu, P. Audebert, P. Georges, and F. Druon, *Opt. Lett.* **42**, 3530 (2017).
- [5] L. Yu, Y. Xu, Y. Liu, Y. Li, S. Li, Z. Liu, W. Li, F. Wu, X. Yang, Y. Yang, C. Wang, X. Lu, Y. Leng, R. Li, and Z. Xu, *Opt. Express* **26**, 2625 (2018).
- [6] H. Kiriya, A. S. Pirozhkov, M. Nishiuchi, Y. Fukuda, K. Ogura, A. Sagisaka, Y. Miyasaka, M. Mori, H. Sakaki, N. P. Dover, K. Kondo, J. K. Koga, T. Z. Esirkepov, M. Kando, and K. Kondo, *Opt. Lett.* **43**, 2595 (2018).
- [7] M. A. Alkhimova, A. Y. Faenov, I. Y. Skobelev, T. A. Pikuz, M. Nishiuchi, H. Sakaki, A. S. Pirozhkov, A. Sagisaka, N. P. Dover, K. Kondo, K.



- 1 Ogura, Y. Fukuda, H. Kiriya, K. 47
- 2 Nishitani, T. Miyahara, Y. Watanabe, 48
- 3 S. A. Pikuz, M. Kando, R. Kodama, 49
- 4 and K. Kondo, *Opt. Express* **25**, 29501 50
- 5 (2017). 51
- 6 [8] J. Nuckolls, L. Wood, A. Thiessen, and 52
- 7 G. Zimmerman, *Nature* **239**, 139 53
- 8 (1972). 54
- 9 [9] R. Betti and O. A. Hurricane, *Nat.* 55
- 10 *Phys.* **12**, 435 (2016). 56
- 11 [10] W. Seka, J. -L. Schwob, and C. Breton, 57
- 12 *J. Appl. Phys.* **42**, 315 (1971). 58
- 13 [11] F. C. Young, R. R. Whitlock, R. 59
- 14 Decoste, B. H. Ripin, D. J. Nagel, J. A. 60
- 15 Stamper, J. M. McMahon, and S. E. 61
- 16 Bodner, *Appl. Phys. Lett.* **30**, 45 62
- 17 (1977). 63
- 18 [12] B. Yaakobi and T. C. Bristow, *Phys.* 64
- 19 *Rev. Lett.* **38**, 350 (1977). 65
- 20 [13] D. Riley, J. J. Angulo-Gareta, F. Y. 66
- 21 Khattak, M. J. Lamb, P. S. Foster, E. J. 67
- 22 Divall, C. J. Hooker, A. J. Langley, R. 68
- 23 J. Clarke, and D. Neely, *Phys. Rev. E* 69
- 24 **71**, 016406 (2005). 70
- 25 [14] K. B. Wharton, C. D. Boley, A. M. 71
- 26 Komashko, A. M. Rubenchik, J. 72
- 27 Zweiback, J. Crane, G. Hays, T. E. 73
- 28 Cowan, and T. Ditmire, *Phys. Rev. E* 74
- 29 **64**, 025401 (2001). 75
- 30 [15] A. L. Kritcher, P. Neumayer, M. K. 76
- 31 Urry, H. Robey, C. Niemann, O. L. 77
- 32 Landen, E. Morse, and S. H. Glenzer, 78
- 33 *High Energy Density Phys.* **3**, 156 79
- 34 (2007). 80
- 35 [16] S. N. Chen, G. Gregori, P. K. Patel, H.- 81
- 36 K. Chung, R. G. Evans, R. R. Freeman, 82
- 37 E. Garcia Saiz, S. H. Glenzer, S. B. 83
- 38 Hansen, F. Y. Khattak, J. A. King, A. 84
- 39 J. Mackinnon, M. M. Notley, J. R. 85
- 40 Pasley, D. Riley, R. B. Stephens, R. L. 86
- 41 Weber, S. C. Wilks, and F. N. Beg, 87
- 42 *Phys. Plasmas* **14**, 102701 (2007). 88
- 43 [17] C. N. Danson, P. A. Brummitt, R. J. 89
- 44 Clarke, J. L. Collier, B. Fell, A. J. 90
- 45 Frackiewicz, S. Hancock, S. Hawkes, 91
- 46 C. Hernandez-Gomez, P. Holligan, M. 92
- H. R. Hutchinson, A. Kidd, W. J. 93
- Lester, I. O. Musgrave, D. Neely, D. R. 94
- Neville, P. A. Norreys, D. A. Pepler, 95
- C. J. Reason, W. Shaikh, T. B. 96
- Winstone, R. W. W. Wyatt, and B. E. 97
- Wyborn, *Nucl. Fusion* **44**, S239 98
- (2004). 99
- [18] I. Y. Skobelev, S. N. Ryazantsev, D. 100
- D. Arich, P. S. Bratchenko, A. Y. 101
- Faenov, T. A. Pikuz, P. Durey, L. 102
- Doehl, D. Farley, C. D. Baird, K. L. 103
- Lancaster, C. D. Murphy, N. Booth, C. 104
- Spindloe, P. McKenna, S. B. Hansen, 105
- J. Colgan, R. Kodama, N. Woolsey, 106
- and S. A. Pikuz, *Photonics Res.* **6**, 234 107
- (2018). 108
- [19] G. Doumy, F. Quéré, O. Gobert, M. 109
- Perdrix, P. Martin, P. Audebert, J. C. 110
- Gauthier, J.-P. Geindre, and T. 111
- Wittmann, *Phys. Rev. E* **69**, 026402 112
- (2004). 113
- [20] R. Hörlein, B. Dromey, D. Adams, Y. 114
- Nomura, S. Kar, K. Markey, P. Foster, 115
- D. Neely, F. Krausz, G. D. Tsakiris, 116
- and M. Zepf, *New J. Phys.* **10**, 083002 117
- (2008). 118
- [21] C. Hernandez-Gomez, in *CLF Annu.* 119
- Rep. 2016-2017* (2017), pp. 6–8. 120
- [22] A. Y. Faenov, S. A. Pikuz, A. I. Erko, 121
- B. A. Bryunetkin, V. M. Dyakin, G. V. 122
- Ivanenkov, A. R. Mingaleev, T. A. 123
- Pikuz, V. M. Romanova, and T. A. 124
- Shelkovenko, *Phys. Scr.* **50**, 333 125
- (1994). 126
- [23] M. A. Alkhimova, I. Y. Skobelev, A. 127
- Y. Faenov, D. A. Arich, T. A. Pikuz, 128
- and S. A. Pikuz, *Quantum Electron.* 129
- 48**, 749 (2018). 130
- [24] C. R. Stillman, P. M. Nilson, S. T. 131
- Ivancic, I. E. Golovkin, C. Mileham, I. 132
- A. Begishev, and D. H. Froula, *Phys.* 133
- Rev. E* **95**, 063204 (2017). 134
- [25] J. J. MacFarlane, I. E. Golovkin, P. R. 135
- Woodruff, D. R. Welch, B. V. Oliver, 136
- T. A. Mehlhorn, and R. B. Campbell, 137
- in *Proc. Third Inert. Conf. Inert.* 138

1        *Fusion Sci. Appl. 2003* (2003), pp. 1–  
2        4.  
3 [26] J. J. MacFarlane, I. E. Golovkin, P.  
4        Wang, P. R. Woodruff, and N. A.  
5        Pereyra, *High Energy Density Phys.* **3**,  
6        181 (2007).  
7 [27] A. S. Martynenko, I. Y. Skobelev, and  
8        S. A. Pikuz, *Appl. Phys. B* **125**, 31  
9        (2019).  
10